The Influence of Vibrational Excitation and Nuclear Dynamics in Multiphoton Photoelectron Circular Dichroism of Fenchone

Dhirendra P. Singh[a), James O.F. Thompson, Katharine L. Reid, Ivan Powis]*

School of Chemistry, The University of Nottingham, University Park, Nottingham NG7 2RD, UK

[a)] Current address: IMEC, Kapeldreef 75, 3001 Leuven, Belgium

*Corresponding Author:

      Email: ivan.powis@nottingham.ac.uk

      Phone: +44 115 9513467

ORCIDs:
      DPS 0000-0002-8855-0597
      JOFT 0000-0003-2720-2692
      KLR 0000-0002-5480-9708
      IP 0000-0002-7941-9079

ABSTRACT

We report photoelectron circular dichroism of S-(+)-fenchone enantiomers recorded with state-state vibrational level resolution using picosecond laser (2+1) resonance enhanced multiphoton ionization via $3s$ and $3p$ Rydberg intermediate states. The $3p$ state decays to the $3s$ state on a picosecond timescale so that, above the $3p$ Rydberg excitation threshold, ionization of vibrationally hot $3s$ states competes with direct $3p^{-1}$ ionization. Complex vibronic dynamics of the $3p{\rightarrow}3s$ internal conversion weaken the Rydberg $\Delta v=0$ propensity rule in both the $3p^{-1}$ and $3s^{-1}$ ionization channels. Large variations of the forward-backward chiral asymmetry factors are observed between $\Delta v=0$ and $\Delta v>0$ vibrational transitions, including dramatic swings from up to ±17%. Such changes of sign indicate complete reversal of the preferred direction for photoelectron emission in the laboratory frame, associated to vibrational motion. These asymmetry switches easily exceed the amplitude and frequency of such vibrationally induced flips previously observed in single photon ionization.

TOC GRAPHIC
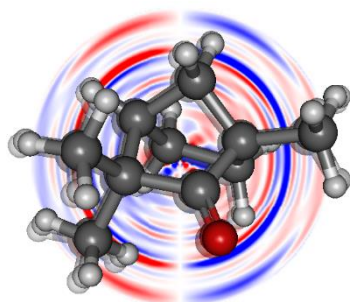
KEYWORDS Chirality; Photoionization; Photoelectron Angular Distributions; Vibronic Interactions;

Photoionization of randomly oriented enantiomers by circularly polarized radiation produces a forward-backward asymmetry in the angular distribution of emitted photoelectrons characterized by Kuhn chiral asymmetry factors, g, that typically range from a few % to several tens %. These asymmetries exceed those typically encountered with traditional single-photon chiroptical techniques by orders of magnitude due to originating in the pure electric dipole approximation.[1, 2] Initially studied using synchrotron radiation in soft X-Ray and vacuum ultraviolet (VUV), this chiral sensitivity has enabled the technique of Photoelectron Circular Dichroism (PECD) as a new probe of molecular orbital structure, configuration, conformation, and clustering.[3-4] The more recent combination of laser excitation sources with PECD[5-6] has opened up further avenues for the investigation of both fundamental light-matter interactions[7, 8, 9-10] and practical analytical applications.[11-15] Resonantly enhanced multiphoton ionization (REMPI) photoelectron circular dichroism (MP-PECD) has received particular interest in both these contexts. Theoretical models have established the premise that in the perturbative limit, MP-PECD can be considered as a photoionization from the optically aligned intermediate state.[6, 16, 17] In principle then, spectroscopic preparation of the resonant state provides a convenient opportunity to state-select and characterize an initial state for the subsequent photoionization step.

Both experimental[7, 13, 18-21] and theoretical[16-17] studies have addressed some aspects of the part played by the intermediate state in MP-PECD, such as its electronic character, degree of alignment, and competing relaxation processes, using the benchmark molecule fenchone ($C_{10}H_{16}O$). However, rather limited attention has been given to the explicit role of vibrational excitation.[20] A dramatic finding from VUV PECD studies was that photoelectron asymmetries of several % in vibrationally cold chiral oxiranes could be caused to completely flip direction by an accompanying weak excitation of certain vibrational modes in the cations.[22-23] Similar behaviour has been reported in PECD of jet-cooled chiral terpenes[24-25] but has yet to be corroborated in MP-PECD.
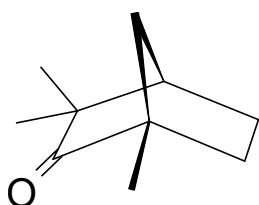
Scheme 1: S-(+)-fenchone

In the following we report a two-photon resonant, one-photon ionization (2+1) MP-PECD investigation of jet cooled S-(+)-fenchone via its 3s, 3p Rydberg states. Using a picosecond (ps) laser we retain sufficient photon resolution to selectively populate distinct vibrational levels in the intermediate state excitation, with comparable resolution for the detection of ion state vibrational excitation in the photoelectron spectrum (PES). We show that the magnitude, and indeed direction, of the MP-PECD asymmetries display a clear dependence on the levels of vibronic excitation.

Figure 1 presents a ps laser (2+1) REMPI spectrum of the 3s and 3p bands (also referred to[26] as the B and C bands) of fenchone.[27] The resolution, estimated from the two-fold convolution of the 1.3 ps laser pulse width is ~17 cm^{-1}. With 75 normal modes, fenchone's vibrational density of states increases very rapidly with energy, leading to highly congested spectra. An investigation of a higher resolution (~0.1 cm^{-1}) REMPI spectrum recorded with a ns laser source has concluded that transitions can be assigned to single vibrational eigenstates only for the first 300 cm^{-1} (40 meV) above the 3s origin.[20] Nevertheless, the experimental spectra in Fig. 1 clearly show significant resolvable vibrational structures ranging across much of the 3s and 3p bands, as confirmed by the Franck Condon simulations for these bands[27] shown in Fig. 1.
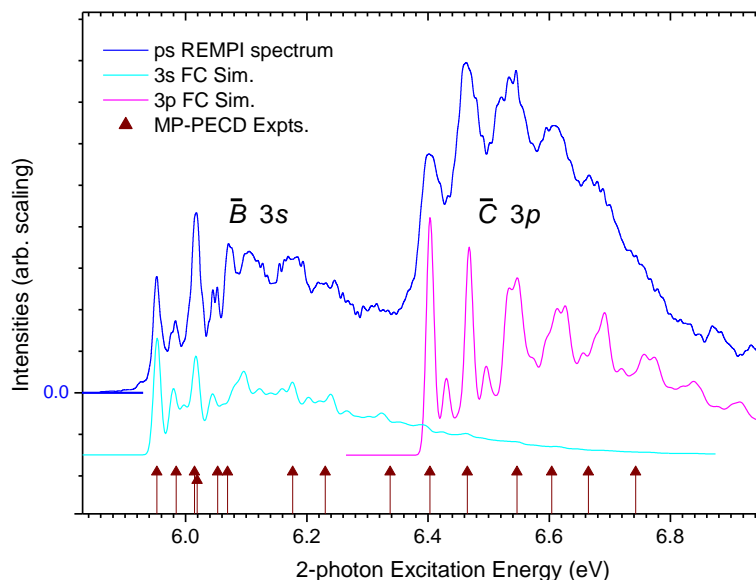
Figure 1. Picosecond laser REMPI spectrum of the 3s/3p bands of fenchone, taken from Ref. [27]. The 3s and 3p$_y$ Franck-Condon simulated vibrational spectra for excitation from the ground state neutral fenchone are taken from the same source. Marked along the bottom are the excitation energies where MP-PECD measurements were recorded.

We have recorded ps REMPI PES and MP-PECD spectra at excitation energies that were primarily chosen to coincide with these vibrational peaks; these energies are marked in Fig. 1. An overview of these results is provided in Figure 2. The two distinctive PES "ridges" running diagonally across the waterfall plot (Fig. 2a) have been previously noted in experiments with nanosecond,[20] picosecond,[27] and femtosecond[19] laser sources. The first ridge, formed following excitation in the *B* band, is identified as arising from 3s state ionization following a strong Δv=0 propensity rule, as expected for Rydberg state ionization. This "3s" PES ridge extends through the subsequent *C* band excitation region, where it is paralleled by a second 3p ionization ridge.

For the present results, the ionization energy of the peak maxima in both the 3s and 3p ridges varies linearly with two-photon excitation energy (Fig. 2c) with fitted slopes of 1.03±0.01 and 0.99±0.03 respectively, indicating that two-photon energy in excess of the threshold, deposited in the Rydberg state, is fully retained as internal energy to the cation. Back extrapolation of the 3s fit to the 8.49 eV adiabatic ionization energy of fenchone[27-28] yields an intercept of 5.965 eV, in very good agreement with the spectroscopically determined $n\rightarrow$3s transition origin of 5.952 eV.[28-29] Similarly, the 3p ridge extrapolates to an intercept of 6.403 eV, corresponding closely with the first intense maximum observed in the 3p excitation region (Fig. 1). These fitting results, and the extremely similar Franck-Condon (FC) simulations calculated for the $S_0 \rightarrow$3s, 3p, and D_0 (cation) excitations,[27] support the identification of these ridges as vibrational energy conserving "Δv=0" transitions.
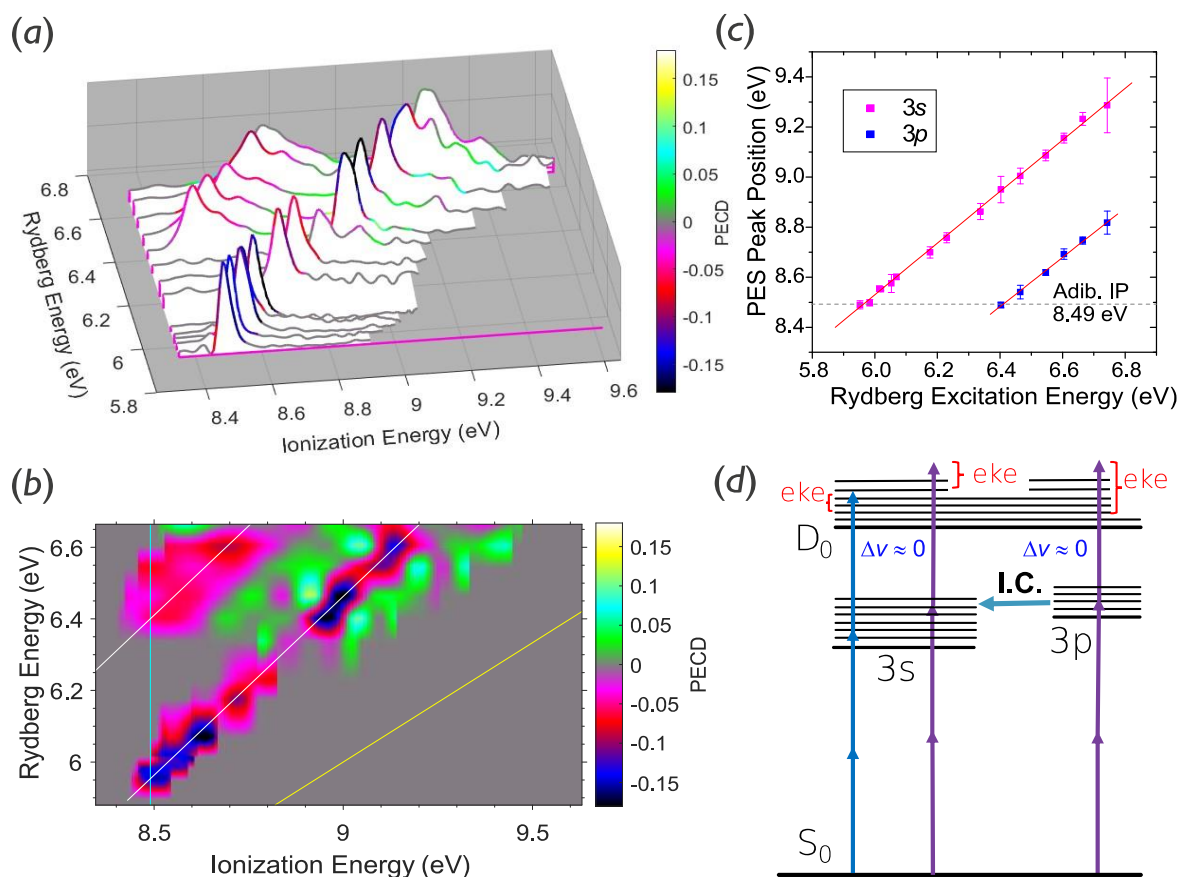
Figure 2 (a) Waterfall plot representing the variation of the set of linearly polarized, (2+1) REMPI PES with increasing two-photon excitation energy. Ionization energy is obtained as the three-photon excitation energy less the electron kinetic energy. Individual spectra have been normalized to the same maximum intensity. The corresponding MP-PECD values are revealed as pseudo-colors draped onto the PES peaks; (b) projection of the MP-PECD using the same pseudo-color mapping. The adiabatic ionization potential (8.49 eV) is marked as solid line while the maximum ionization energy accessible in a three-photon process is indicated by a yellow dash-dotted line. Dashed lines indicate the variation of the PES principal peak positions seen as ridges in the waterfall plot; (c) Plot to show variation with ionization energy of the principal ($\Delta v=0$) PES peak position along the 3s and 3p ridges; (d) Schematic showing (2+1) REMPI excitation. The transitions marked terminate at the 3-photon energy but indicate the vibration level-preserving electron energy release given the $\Delta v=0$ propensity for Rydberg ionization.

Above the 3p excitation threshold the relative intensity of the ridges was already known to depend on the excitation pulse duration, with the 3p ionization dominating the fs spectra,[19] while the 3s dominates in the ns regime. From these previous observations, an internal conversion from the 3p to 3s state, with an intermediate lifetime, was inferred.[20] A schematic of this proposed (2+1) REMPI excitation scheme is given in Fig. 2d. Energetically, ionization via both 3p and 3s intermediate states is possible above the 3p excitation threshold. However, already at this threshold the FC factors for direct excitation S$_0$→3s are unfavourable (see FC vibrational simulations in Fig. 1).[27] Additionally, we note the relative intensities of the "3s" and 3p PES peaks are the same whether recorded with linear (Fig. 2a) or circular (Fig. 7 Ref. [27]) polarizations. An experimental/computational investigation of circular-linear dichroism in fenchone shows that, relative to the C band 3p Rydberg excitations, the

two-photon transition strength for the 3s electronic excitation is approximately 50% greater with circular polarization, but 50% less with linear polarization.[27] The failure to observe changed 3s^{-1}:3p^{-1} PES peak intensity ratios with linear and circular polarizations implies that both 3s^{-1} and 3p^{-1} ionization channels proceed via excitation of a common electronic intermediate. This further corroborates the inferred 3p→3s internal conversion as the dominant 3s excitation mechanism in the C band region.

The single narrow 3s^{-1} PES peak shapes recorded via direct 3s Rydberg excitation in the B band change appearance when excitation occurs via the C band. Both the 3s^{-1} and, now, the 3p^{-1} PES peaks are broad and structured (Fig. 2a). While in each ionization channel the Δv=0 ionization remains the most intense component, the additional structures have previously been attributed to additional vibrational excitation in both 3p^{-1} and 3s^{-1} ionization channels — see for example Fig. 12 Ref. [27]. Such weakening of the Δv=0 propensity is indicative of more complex vibrational dynamics associated with the 3p→3s conversion and strong vibronic coupling of the 3s and 3p potential surfaces.
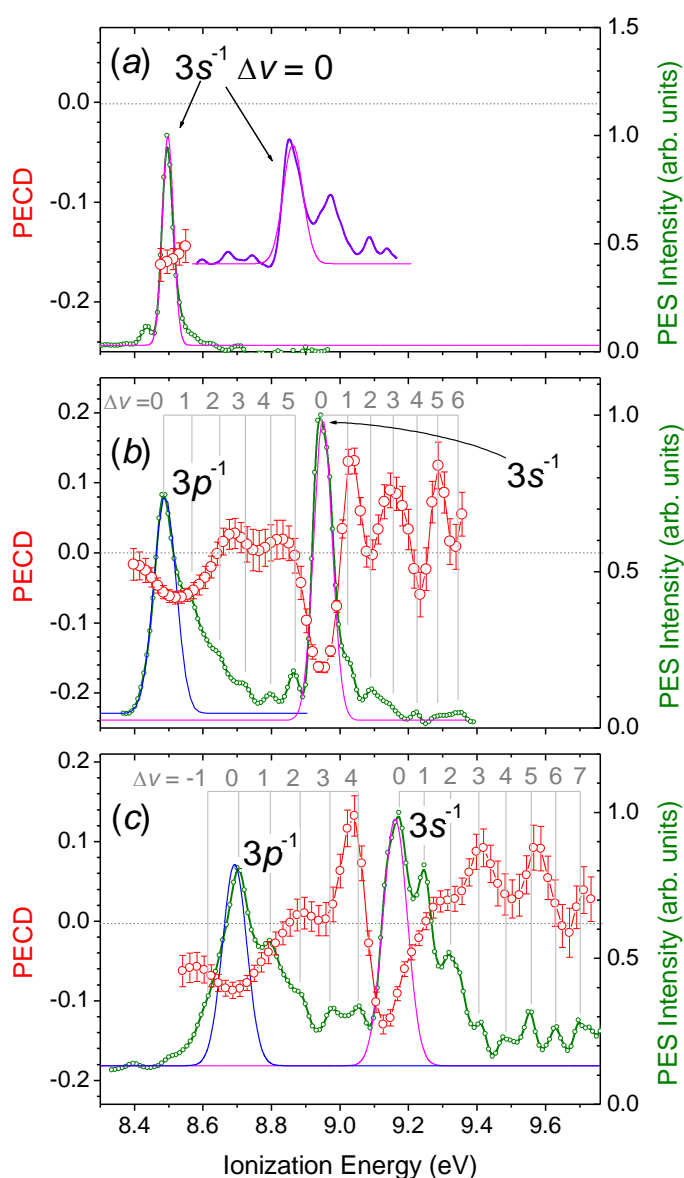
Figure 3. MP-PECD spectra (red) measured at (a) 5.98 eV (b) 6.40 eV (c) 6.60 eV two-photon excitation energies. Corresponding linear polarized PES measurements are plotted in green. Additionally, panel (a) includes 6.34 eV measurements, plotted in red and violet on the same axes. For clarity only a single indicative error bar is drawn here. Best fit Gaussian functions for the 3s (magenta) and 3p (blue) Δv=0 PES component peaks are included. For the 3p C band excitations (b) and (c), the vibrational features identifiable from the PES are marked, helping reveal correlations with the PECD. (Further examples appear in Supplementary Information.)

An overview of the present MP-PECD results is provided as pseudo-color mapping in Fig. 2a,b with examples of individual PES and MP-PECD spectra in Figure 3. For an overall three photon process the PECD forward-backward asymmetry can be defined and evaluated as $PECD = 2b_1^{lcp} - \frac{1}{2}b_3^{lcp} + \frac{1}{4}b_5^{lcp}$, where b_j^{lcp} are the coefficients of the jth Legendre polynomial term in the left circularly polarized (*lcp*) photoelectron angular distribution.[6, 30] These odd Legendre terms are antisymmetric with respect to the forward-backward direction of the light beam.

The 3*s* and 3*p* PES ridges are evident as local minima in the *PECD* values recorded along the Δv=0 peaks but, above the 3*p* Rydberg excitation threshold, both the 3*s* and 3*p* *PECD* swing from negative to positive values as the ionization energy (vibrational excitation) increases above the Δv=0 peaks. These swings, of as much as ±17%, show the strong forward-backward photoelectron scattering asymmetry undergoing a complete reverse in preferred direction. As seen in Fig. 3, there is a correlation between the PECD spectra and identifiable vibrational structure in the PES, and we conclude that there is here a clear vibrational influence on the PECD. The consistency and amplitude of these oscillations dramatically exceeds previous observations of vibrationally flipped PECD[22-25] and is the principal finding of this study.

In fact, a swing from negative to positive *PECD* in the 3*p*[-1] ionization of fenchone was noted by Kastner et al.[19] However, the much greater bandwidth of their 25 fs laser excitation precluded the observation of the vibrational structure as revealed here, and so it was tentatively suggested that two different, unresolved 3*p* states (separation ~120 meV) underlying the rather symmetrical PES band profile could be responsible. [19-20] No such switch in the asymmetry was previously remarked in the 3*s*[-1] PES bands.

Our measurements include one made at an excitation energy of 6.34 eV, just below the observed REMPI C band. The signal level is low in this region, and a substantial background is evident in the REMPI PES (Fig. 3a). Two relatively narrow but partially overlapped PES peaks are seen, the first of which fits perfectly the trends established by the 3*s* Δv=0 PES ridge (Fig. 2) and which we therefore assign as such. The second lies ~0.11 eV to higher energy (and a third, similarly spaced, may possibly be discerned from the noise above that). This spacing does not match other fenchone vibrational features and an assignment of this additional feature is uncertain.

To facilitate comparison with previous studies that could only identify Δv=0 ionizations, we isolate and extract PECD asymmetries across the principal Δv=0 peaks in the 3*s* and 3*p* ridges that are observed here, and plot their mean values in Fig. 4. For spectra recorded across the first halves of both the *B* 3*s* and *C* 3*p* Rydberg excitation bands, the 3*s* Δv=0 *PECD* values are in agreement with previous ns and fs experiments, [19-20] starting at approximately -17±3 % in the *B* band and reducing in magnitude to less than -10% in the shortest wavelength C band excitations. On the other hand, the *PECD* values recorded between 6.15 –6.35 eV excitation have a significantly lesser magnitude than either the ns or fs results. The reasons for this discrepancy are unclear but may be associated with the differing times available for relaxation and IVR in the 3*s* intermediate. A 3.3 ps lifetime for the 3*s*

state has been deduced from direct pump-probe measurements, and a faster 400 fs decay time was associated with unspecified IVR or dephasing in the 3*s* state.[21]

The $3p^{-1}$ *PECD* magnitudes (Fig. 4) are significantly larger (~ -5%) than were reported using a femtosecond laser source.[19] In large part we attribute that to an ability to better identify and isolate the Δv=0 contribution with the better resolved ps PES measurements, so avoiding averaging with the opposite sign contributions that accompany higher vibrational excitations in the ion state. Even so, we confirm a marked difference between the PECD resulting from direct Δv=0 ionization from the 3*p* Rydberg states and that from ionization of the 3*s* state, whether accessed by direct excitation or following internal conversion from the 3*p* states.
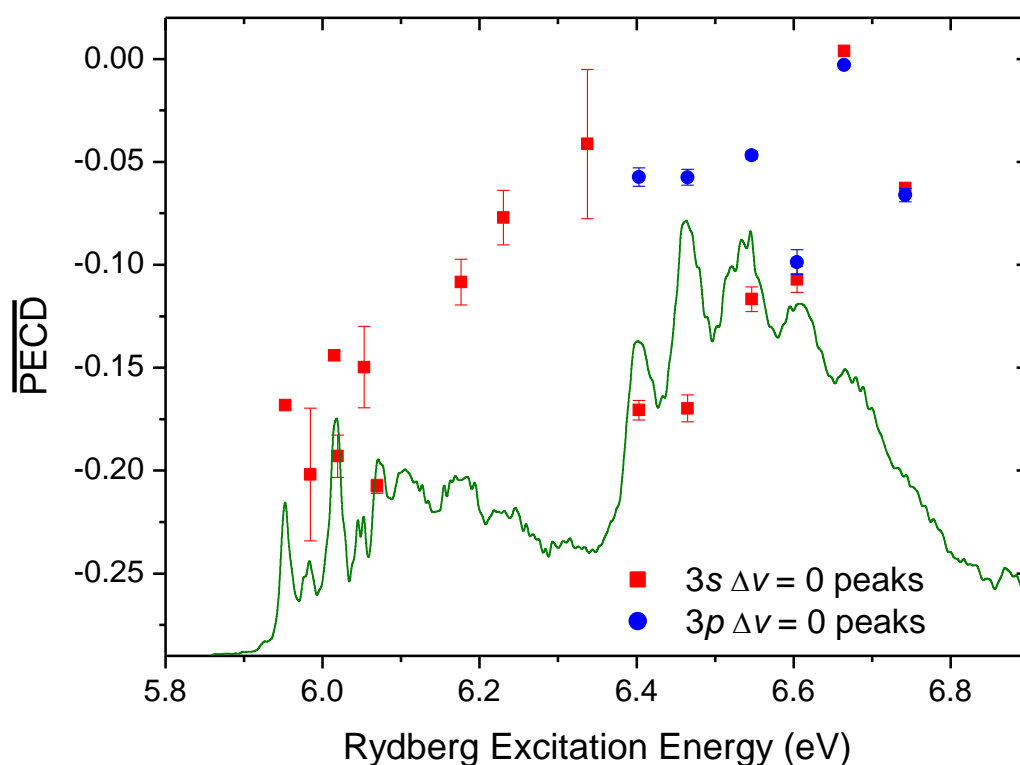
Figure 4 Mean Δv=0 PECD asymmetries (baseline corrected) for $3s^{-1}$ and $3p^{-1}$ ionizations. These are weighted averages formed across the FWHM of gaussian functions previously fitted to the principal Δv=0 PES peaks (shown in Fig. 3). For reference, the ps REMPI spectrum, with arbitrarily scaled intensity, is shown in green.

These results show how a degree of vibrational selectivity in both the ionized and the ionizing states could be exploited to examine vibrationally influenced chiral photoionization dynamics by selective excitation of the neutral intermediate state with picosecond MP-PECD. Earlier conclusions[7, 20] that there is no substantial vibrational influence on fenchone MP-PECD need to be qualified by restriction to $3s^{-1}$ Δv=0 transitions only. Clearly, the ionization with additional ion vibrational excitation observed (Figs. 2, 3) in the transition $S_0 \rightarrow 3p \xrightarrow{I.C.} 3s \rightarrow D_0$ reflects more complex vibrational dynamics with dramatic consequences for the PECD asymmetry, including a complete flip in

direction as was observed, more weakly, in some VUV studies.[22-25] Moreover, the similar observation of propensity rule violating $\Delta v{\neq}0$ ionization in the $3p^{-1}$ channel, with again a corresponding reversal in the chiral photoelectron asymmetry, is very likely a demonstration that the evolution of the initially excited $3p$ vibrational wavepacket occurs over both of the non-adiabatically coupled Rydberg surfaces. We may anticipate that complementing such experiments with theoretical modelling will provide fresh insight into the vibronic dynamics and $3p$ Rydberg state predissociation. Such work is in progress.

Quite aside from the intrinsic interest of the coupled electron-nuclear dynamics observed by MP-PECD, these results also suggest caution when interpreting or using PECD asymmetry measurements, for example for determining enantiomeric excess,[11-13] without resolving or otherwise fully characterizing/controlling the vibrational populations of both initial and final states.

Experimental Method

Our experimental apparatus and method has been described elsewhere.[27, 31]   Briefly, the picosecond laser system consists of a Ti:Sapphire oscillator, regenerative amplifier, and single-pass amplifier chain (Coherent) pumping an optical parametric amplifier (Light Conversion, TOPAS) providing a 1kHz pulse train between 350–450 nm (~ 10–20 uJ). The pulse duration of 1.3 ps corresponds to a transform limited bandwidth 11.3 cm^{-1}. Polarization control of the uv output was performed by half- and quarter-waveplates in the beam path. The degree of circular polarization obtained for PECD experiments was confirmed by measurement of the Stokes S_3 parameter to be always >96%.

He (1 bar) was bubbled through a room temperature commercial sample (Sigma-Aldrich) of S-(+)-fenchone enantiomer and admitted into a velocity map imaging (VMI) electron spectrometer[31] by expansion through a 1kHz pulsed valve (Amsterdam ACPV2, 150 μm nozzle). The seeded molecular beam is then skimmed before entering the main spectrometer chamber. Typical operating pressures were $2{\times}10^{-7}$ mbar, with a background pressure of $5{\times}10^{-8}$ mbar. The laser was focussed into this chamber by a 30 cm lens, providing intensities estimated as 10^{11}–10^{12} W cm^{-2} in the ionization region.

The VMI photoelectron 2D images were analysed to obtain PES and, for circular polarizations, PECD spectra by Abel inversion,[32] following a previously described procedure[33] (examples provided in Supplementary Information). When forming the LCP-RCP difference images the image pixels were re-binned prior to inversion to improve the PECD statistics, at the expense of a slightly reduced kinetic energy resolution compared with the linear polarized PES. In regions of low PES intensity, where the noise in forming the difference signal and its intensity-normalization becomes excessive, PECD plotting is suppressed. The $\Delta v{=}0$ PES peaks were fitted with gaussian functions. Above the 3p excitation threshold the widths were constrained to be within 10% of the extrapolated widths of the pure $\Delta v{=}0$ peaks in the 3s excitation region. While not unique, these fits help visualise the isolated $\Delta v{=}0$ components when the peak shapes are asymmetrically broadened by further vibrational excitation (see Fig. 3). Characteristic PECD values for the $\Delta v{=}0$ peaks, plotted in Fig. 4, are obtained as weighted averages formed across the fitted gaussian's FWHM.

Acknowledgements

Supplementary Information:

- C band (3p) excitation REMPI PES/MP-PECD: Further Examples.
- VMI Image Analysis

References

1.   Ritchie, B. Theory of the angular distribution of photoelectrons ejected from optically active molecules and molecular negative ions. *Phys. Rev. A* **1976,** *13*, 1411-1415.
2.   Powis, I. Photoelectron circular dichroism of the randomly oriented chiral molecules glyceraldehyde and lactic acid. *J. Chem. Phys.* **2000,** *112* (1), 301-310.
3.   Nahon, L.; Garcia, G. A.; Powis, I. Valence shell one-photon photoelectron circular dichroism in chiral systems. *J. Electron Spectrosc. Relat. Phenom.* **2015,** *204* (B), 322-334.
4.   Turchini, S. Conformational effects in photoelectron circular dichroism. *Journal of Physics: Condensed Matter* **2017,** *29* (50), 503001.
5.   Lux, C.; Wollenhaupt, M.; Bolze, T.; Liang, Q. Q.; Kohler, J.; Sarpe, C.; Baumert, T. Circular Dichroism in the Photoelectron Angular Distributions of Camphor and Fenchone from Multiphoton Ionization with Femtosecond Laser Pulses. *Angew. Chem.-Int. Edit.* **2012,** *51* (20), 5001-5005.
6.   Lehmann, C. S.; Ram, N. B.; Powis, I.; Janssen, M. H. M. Imaging photoelectron circular dichroism of chiral molecules by femtosecond multiphoton coincidence detection. *J. Chem. Phys.* **2013,** *139* (23), 234307.
7.   Beaulieu, S.; Comby, A.; Fabre, B.; Descamps, D.; Ferré, A.; Garcia, G.; Géneaux, R.; Légaré, F.; Nahon, L.; Petit, S.; Ruchon, T.; Pons, B.; Blanchet, V.; Mairesse, Y. Probing ultrafast dynamics of chiral molecules using time-resolved photoelectron circular dichroism *Faraday Discuss.* **2016,** *194*, 325-348.
8.   Beaulieu, S.; Ferre, A.; Geneaux, R.; Canonge, R.; Descamps, D.; Fabre, B.; Fedorov, N.; Legare, F.; Petit, S.; Ruchon, T.; Blanchet, V.; Mairesse, Y.; Pons, B. Universality of photoelectron circular dichroism in the photoionization of chiral molecules. *New J. Phys.* **2016,** *18*, 102002.
9.   Beaulieu, S.; Comby, A.; Clergerie, A.; Caillat, J.; Descamps, D.; Dudovich, N.; Fabre, B.; Géneaux, R.; Légaré, F.; Petit, S.; Pons, B.; Porat, G.; Ruchon, T.; Taïeb, R.; Blanchet, V.; Mairesse, Y. Attosecond-resolved photoionization of chiral molecules. *Science* **2017,** *358* (6368), 1288-1294.
10.   Demekhin, P. V.; Artemyev, A. N.; Kastner, A.; Baumert, T. Photoelectron Circular Dichroism with Two Overlapping Laser Pulses of Carrier Frequencies omega and 2 omega Linearly Polarized in Two Mutually Orthogonal Directions. *Phys. Rev. Lett.* **2018,** *121* (25).
11.   Rafiee Fanood, M. M.; Ram, N. B.; Lehmann, C. S.; Powis, I.; Janssen, M. H. M. Enantiomer specific analysis of multi-component mixtures by correlated electron imaging–ion mass spectrometry *Nat. Commun.* **2015,** *6*, 7511.
12.   Kastner, A.; Lux, C.; Ring, T.; Zullighoven, S.; Sarpe, C.; Senftleben, A.; Baumert, T. Enantiomeric Excess Sensitivity to Below One Percent by Using Femtosecond Photoelectron Circular Dichroism. *ChemPhysChem* **2016,** *17* (8), 1119-1122.
13.   Comby, A.; Bloch, E.; Bond, C. M. M.; Descamps, D.; Miles, J.; Petit, S.; Rozen, S.; Greenwood, J. B.; Blanchet, V.; Mairesse, Y. Real-time determination of enantiomeric and isomeric content using photoelectron elliptical dichroism. *Nat. Commun.* **2018,** *9*, 5212.
14.   Miles, J.; Fernandes, D.; Young, A.; Bond, C. M. M.; Crane, S. W.; Ghafur, O.; Townsend, D.; Sá, J.; Greenwood, J. B. A new technique for probing chirality via photoelectron circular dichroism. *Analytica Chimica Acta* **2017,** *984*, 134-139.
15.   Kruger, P.; Weitzel, K. M. Photoelectron Circular Dichroism in the Photodetachment of Amino Acid Anions. *Angew. Chem.-Int. Edit.* **2021,** *60*, 17861-17865.
16.   Goetz, R. E.; Isaev, T. A.; Nikoobakht, B.; Berger, R.; Koch, C. P. Theoretical description of circular dichroism in photoelectron angular distributions of randomly oriented chiral molecules after multi-photon photoionization. *J. Chem. Phys.* **2017,** *146* (2), 024306.
17.   Muller, A. D.; Artemyev, A. N.; Demekhin, P. V. Photoelectron circular dichroism in the multiphoton ionization by short laser pulses. II. Three- and four-photon ionization of fenchone and camphor. *J. Chem. Phys.* **2018,** *148* (21), 214307.

18.   Lux, C.; Wollenhaupt, M.; Sarpe, C.; Baumert, T. Photoelectron Circular Dichroism of Bicyclic Ketones from Multiphoton Ionization with Femtosecond Laser Pulses. *ChemPhysChem* **2015,** *16* (1), 115-137.

19.   Kastner, A.; Ring, T.; Kruger, B. C.; Park, G. B.; Schafer, T.; Senftleben, A.; Baumert, T. Intermediate state dependence of the photoelectron circular dichroism of fenchone observed via femtosecond resonance-enhanced multi-photon ionization. *J. Chem. Phys.* **2017,** *147* (1), 013926.

20.   Kastner, A.; Koumarianou, G.; Glodic, P.; Samartzis, P. C.; Ladda, N.; Ranecky, S. T.; Ring, T.; Vasudevan, S.; Witte, C.; Braun, H.; Lee, H.-G.; Senftleben, A.; Berger, R.; Park, G. B.; Schäfer, T.; Baumert, T. High-resolution resonance-enhanced multiphoton photoelectron circular dichroism. *Phys. Chem. Chem. Phys.* **2020,** *22* (14), 7404-7411.

21.   Comby, A.; Beaulieu, S.; Boggio-Pasqua, M.; Descamps, D.; Legare, F.; Nahon, L.; Petit, S.; Pons, B.; Fabre, B.; Mairesse, Y.; Blanchett, V. Relaxation Dynamics in Photoexcited Chiral Molecules Studied by Time-Resolved Photoelectron Circular Dichroism: Toward Chiral Femtochemistry. *J. Phys. Chem. Lett.* **2016,** *7* (22), 4514-4519.

22.   Garcia, G. A.; Nahon, L.; Daly, S.; Powis, I. Vibrationally induced inversion of photoelectron forward-backward asymmetry in chiral molecule photoionization by circularly polarized light. *Nat. Commun.* **2013,** *4*, 2132.

23.   Garcia, G. A.; Dossmann, H.; Nahon, L.; Daly, S.; Powis, I. Identifying and understanding strong vibronic interaction effects observed in the asymmetry of chiral molecule photoelectron angular distributions. *ChemPhysChem* **2017,** *18* (5), 500-512.

24.   Rafiee Fanood, M. M.; Ganjitabar, H.; Garcia, G. A.; Nahon, L.; Turchini, S.; Powis, I. Intense Vibronic Modulation of the Chiral Photoelectron Angular Distribution Generated by Photoionization of Limonene Enantiomers with Circularly Polarized Synchrotron Radiation. *ChemPhysChem* **2018,** *19*, 921-933.

25.   Ganjitabar, H.; Garcia, G.; Nahon, L.; Powis, I. Decoupling Vibration and Electron Energy Dependencies in the Photoelectron Circular Dichroism of a Terpene, 3-carene. *J. Chem. Phys.* **2020,** *153* (3), 034302.

26.   Pulm, F.; Schramm, J.; Hormes, J.; Grimme, S.; Peyerimhoff, S. D. Theoretical and experimental investigations of the electronic circular dichroism and absorption spectra of bicyclic ketones. *Chem. Phys.* **1997,** *224* (2-3), 143-155.

27.   Singh, D. P.; Oliveira, N. D.; Garcia, G.; Vredenborg, A.; Powis, I. Experimental and Theoretical Study of 3sp(d) Rydberg States of Fenchone by Polarized Laser Resonance-Enhanced-Multiphoton-Ionization & Fourier Transform VUV Absorption Spectroscopy. *ChemPhysChem* **2020,** *21*, 2468-2483.

28.   Kastner, A.; Ring, T.; Braun, H.; Senftleben, A.; Baumert, T. Observation of Photoelectron Circular Dichroism Using a Nanosecond Laser. *ChemPhysChem* **2019,** *20* (11), 1416-1419.

29.   Cornish, T. J.; Baer, T. EXPERIMENTAL LINK BETWEEN THE C-13 NMR CHEMICAL-SHIFT OF CARBONYL CARBONS AND THE ENERGY SHIFTS OBSERVED IN THE N- 3S OPTICAL-TRANSITION OF CYCLIC-KETONES. *J. Am. Chem. Soc.* **1988,** *110* (19), 6287-6291.

30.   Janssen, M. H. M.; Powis, I. Detecting chirality in molecules by imaging photoelectron circular dichroism. *Phys. Chem. Chem. Phys.* **2014,** *16* (3), 856-871.

31.   Bellm, S. M.; Reid, K. L. Evaluation of the use of photoelectron imaging in obtaining photoelectron spectra and angular distributions: comparison with the field-free time-of-flight method. *Chem. Phys. Lett.* **2004,** *395* (4-6), 253-258.

32.   Garcia, G. A.; Nahon, L.; Powis, I. Two-dimensional charged particle image inversion using a polar basis function expansion. *Rev. Sci. Inst.* **2004,** *75* (11), 4989-4996.

33.   Ganjitabar, H.; Singh, D. P.; Chapman, R.; Gardner, A.; Minns, R. S.; Powis, I.; Reid, K. L.; Vredenborg, A. The role of the intermediate state in angle-resolved photoelectron studies using (2+1) resonance-enhanced multiphoton ionization of the chiral terpenes, α-pinene and 3-carene. *Mol. Phys.* **2020,** *119* (1-2), e1808907.

Figure Captions

Figure 1. Picosecond laser REMPI spectrum of the 3s/3p bands of fenchone, taken from Ref. [27]. The 3*s* and 3*p_y* Franck-Condon simulated vibrational spectra for excitation from the ground state neutral fenchone are taken from the same source. Marked along the bottom are the excitation energies where MP-PECD measurements were recorded.

Figure 2 (a) Waterfall plot representing the variation of the set of linearly polarized, (2+1) REMPI PES with increasing two-photon excitation energy. Ionization energy is obtained as the three-photon excitation energy less the electron kinetic energy. Individual spectra have been normalized to the same maximum intensity. The corresponding MP-PECD values are revealed as pseudo-colors draped onto the PES peaks; (b) projection of the MP-PECD using the same pseudo-color mapping. The adiabatic ionization potential (8.49 eV) is marked as solid line while the maximum ionization energy accessible in a three-photon process is indicated by a dash-dotted line. Dashed lines indicate the variation of the PES principal peak positions seen as ridges in the waterfall plot; (c) Plot to show variation with ionization energy of the principal (Δv=0) PES peak position along the 3*s* and 3*p* ridges; (d) Schematic showing (2+1) REMPI excitation. The transitions marked terminate at the 3-photon energy but indicate the vibration level-preserving electron energy release given the Δv=0 propensity for Rydberg ionization.

Figure 3. MP-PECD spectra (red) measured at (a) 5.98 eV (b) 6.40 eV (c) 6.60 eV two-photon excitation energies. Corresponding linear polarized PES measurements are plotted in green. Additionally, panel (a) includes 6.34 eV measurements, plotted in red and violet on the same axes. For clarity only a single indicative error bar is drawn here. Best fit Gaussian functions for the 3*s* (magenta) and 3*p* (blue) Δv=0 PES component peaks are included. For the 3*p* C band excitations (b) and (c), the vibrational features identifiable from the PES are marked, helping reveal correlations with the PECD. (Further examples appear in Supplementary Information.)

Figure 4 Mean Δv=0 PECD asymmetries (baseline corrected) for $3s^{-1}$ and $3p^{-1}$ ionizations. These are weighted averages formed across the FWHM of gaussian functions previously fitted to the principal Δv=0 PES peaks (shown in Fig. 3). For reference, the ps REMPI spectrum, with arbitrarily scaled intensity, is shown in green.